2021 IEEE Conference on Control Technology and Applications (CCTA).
August 8-11, 2021. San Diego, California

2021 IEEE Conference on Control Technology and Applications (CCTA).
August 8-11, 2021. San

A solution to gain loss in hybrid integrator-gain systems

M.F. Heertjes S.J.A.M. Van den Eijnden W.P.M.H. Heemels H. Nijmeijer

2021 IEEE Conference on Control Technology and Applications (CCTA) | 978-1-6654-3643-4/21/$31.00 ©2021 IEEE | DOI: 10.1109/CCTA48906.2021.9658966

***Abstract*— Hybrid integrator-gain systems (HIGS) are nonlinear control elements that are designed to primarily operate as integrators in so-called integrator mode. Switching to gain mode occurs only when needed to keep sign equivalence between the input and output signals of the control element, thereby aiming for phase advantages. In order to guarantee the integrator mode to be the primary mode of operation, in this paper a combined pre- and post-filtering approach is studied. Such an approach offers a solution to the problem of gain loss that occurs when the HIGS switches too often between its modes. Typically, this happens in the presence of dominant high-frequency contributions in the input to the HIGS. Along the discussion on pre- and post-filtering, measurement results are presented from a high-performance industrial stage system.**

***Index Terms*— advanced motion control, hybrid integrator-gain systems, nonlinear PID control, wafer scanners.**

I. Introduction

Hybrid integrator-gain systems (abbreviated with HIGS) are nonlinear elements that have been successfully used in PID control [3]. On the basis of these elements, integrators have been synthesized that (from a describing function point of view) have similar magnitude characteristics as simple linear integrators, but with phase advantages of up to 51.85 degrees. This value is also found in reset control systems and relates to the Clegg integrator [11]. Different from reset systems, however, HIGS do not admit discontinuous changes of the integrator states thereby avoiding discontinuities. As such, the study of accumulations of reset times (cf. Zeno behaviour), or avoiding such accumulations by time-regularizations, becomes irrelevant for HIGS [12].

Since the high-precision motion industry primarily uses the frequency domain for its PID control design, dedicated HIGS elements have been developed using frequency-domain reasonings. Examples of such elements are the HIGS lowpass filter [4] and the HIGS-PID controller in [5], the latter exploiting a simple hybrid integrator. Other nonlinear integrators found in the literature, some of which more attuned to time-domain reasonings, are the variable gain integrator in [8], the (filtered) split-path nonlinear integrator in [10], and fractional-order reset control in [2] to name a few. Many nonlinear integrators, if not all, rely on the frequency content of their input in generating effective outputs. That is, in the absence of the superposition principle, high-frequency contributions in the input compromise the ability of the nonlinear integrator to generate sufficient gain in rejecting additionally present low-frequency contributions. To avoid such a gain loss, in this paper a pre- and post-filtering approach [9], [7] is studied for a HIGS. The approach is considered sufficiently generic to allow for extension to various other types of nonlinear integrators, including the ones mentioned earlier.

Corresponding author: Marcel Heertjes is with Eindhoven University of Technology, Department of Mechanical Engineering, Eindhoven, The Netherlands, email: m.f.heertjes@tue.nl, and with ASML, Veldhoven, The Netherlands, email: marcel.heertjes@asml.com

The strictly technological contributions are: (i) a pre- and post-filtering HIGS design, (ii) a measure to conclude if the describing function provides an accurate and thus meaningful description for frequency-domain characterization in the case of multi-sine input, and (iii) measurement results from an industrial stage system that demonstrate the effectiveness of pre- and post-filtering for HIGS-PID control design.

The paper is further organized as follows. In Section II, a brief description of HIGS will be given, which is used in Section III for integrator design. In Section IV, the HIGS is shown to result in gain loss when subjected to a multi-sine input. Section V presents a solution to this problem in the form of pre- and post-filtering. In Section VI, time-series measurements from an industrial stage system are presented. These measurements showcase the effectiveness of the pre- and post filtering when used in a HIGS-PID control design. This paper is concluded with Section VII.

II. Hybrid integrator-gain systems

Consider a simple integrator described in time-domain by $\dot{x} = \omega_i e$, with state x, input e, output $u = x$, integrator frequency ω_i, and the initial condition $x(0) = 0$. In comparison, the piecewise linear system $\mathcal{H}(\cdot)$ referred to as HIGS is defined by

$$\mathcal{H}(\dot{e}, e, u) := \begin{cases} \dot{x}_h &= \omega_h e, \quad \text{if } (\dot{e}, e, u) \in \mathbb{F}_{int} \\ x_h &= k_h e, \quad \text{if } (\dot{e}, e, u) \in \mathbb{F}_{gain} \\ u &= x_h, \end{cases} \tag{1}$$

with state x_h, input e with corresponding time derivative $\dot{e}$, control output u, parameters $\omega_h \in [0, \infty)$ and $k_h \in [0, \infty)$ representing the integrator frequency and gain value, respectively, and with the initial condition $x_h(0) = 0$. Furthermore,

$$\mathbb{F} := \left\{ (e, u) \in \mathbb{R}^2 | eu \geq \frac{1}{k_h} u^2 \right\} \tag{2}$$

indicates the sector in which (1) operates, with $\mathbb{F}_{int}$ and $\mathbb{F}_{gain}$ denoting the sets where either integrator mode (primarily within the sector) or gain mode (on the sector boundary $u = k_h e$) is active, see [3], [5] for more details, namely

$$\mathbb{F}_{int} := \left\{ (\dot{e}, e, u) \in \mathbb{R}^3 | (e, u) \in \mathbb{F} \right\} \setminus \mathbb{F}_{gain}, \tag{3}$$

$$\mathbb{F}_{gain} := \left\{ (\dot{e}, e, u) \in \mathbb{R}^3 | (e, u) \in \mathbb{F} \wedge u = k_h e \wedge \omega_h e^2 > k_h \dot{e} e \right\}. \tag{4}$$

In gain mode the dependency of $\mathcal{H}(\cdot)$ on $\dot{e}$ is shown by $\omega_h e^2 > k_h \dot{e} e$, which assures that HIGS can only switch to integrator mode if its vector field points toward the interior of the sector in (2). $\mathcal{H}$ in (1) is homogeneous in the sense that any constant α multiplied with input e scales the output

Authorized licensed use limited to: Eindhoven University of Technology. Downloaded on April 03,2023 at 18:16:04 UTC from IEEE Xplore. Restrictions apply.

u with the same α, *i.e.*, $\alpha e \mapsto \alpha u$, $\alpha \in \mathbb{R}$. Moreover, $\mathcal{H}$ satisfies $\text{sign}\{e\} = \text{sign}\{u\}$, *i.e.*, its input and output e, u always have equal sign. The latter gives a clear phase advantage over a simple (linear) integrator when evaluated in the frequency domain using its describing function, see for example [3], [5].

III. Hybrid integrator design

In PID control, simple integrators are used for mainly two reasons: (i) to improve low-frequency disturbance rejection properties of the closed-loop system, and (ii) to remove DC error. Regarding the latter, the integrator needs to sustain a DC level of its state x, which is generally not possible with $\mathcal{H}$ in (1). Namely, the value of state x_h (and thus the output u) inevitably becomes zero as soon as the input e reaches zero. This poses a problem, for example, when one needs to levitate a motion system toward a desired levelling position.

To address this issue, consider the hybrid integrator design $\mathcal{C}^{\mathcal{H}}$ as depicted in Fig. 1 with integrator frequency ω_i. Without loss of generality we choose $k_h = 1$ and include this gain later on as part of the loop gain of the overall controller of which $\mathcal{C}^{\mathcal{H}}$ is just a particular element. The extra (simple)

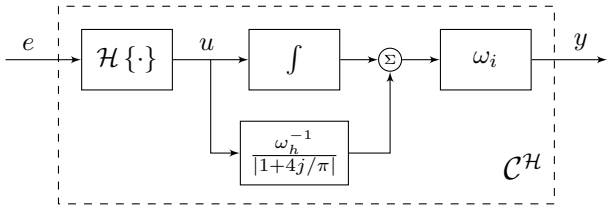

Fig. 1: Block diagram of the HIGS configuration $\mathcal{C}^{\mathcal{H}}$.

integrator ensures that $\mathcal{C}^{\mathcal{H}}$, having two states x_h and x, can sustain a DC output level through its secondary state variable x. The extra forward path with gain $\omega_h^{-1}/|1+4j/\pi|$ is used to ensure that the simple integrator is dominant in the low-frequency range, while $\mathcal{H}$ is dominant in the high-frequency range. The gain value $\omega_h^{-1}/|1+4j/\pi|$ stems from describing function analysis [5], and results in ω_i being the overall gain of the interconnection $\mathcal{C}^{\mathcal{H}}$.

Now consider the simplified multi-sine input e as

$$e(t) = \sin(\omega t) + \epsilon \sin(9\omega t),\ \omega = 2\pi f, \tag{5}$$

with f denoting the base frequency component for which we desire $\mathcal{H}$ to mainly operate in integrator mode, $9f$ a (parasitic) frequency component, and amplitude $\epsilon \in \mathbb{R}_{\geq 0}$. In frequency-domain, the properties of $\mathcal{C}^{\mathcal{H}}$ from Fig. 1 can be studied (to some extent) by its describing function. Namely, for $\mathcal{H}$ in (1) consider the describing function

$$\mathcal{N}^{\mathcal{H}}(j\omega) = a_1(\omega) + jb_1(\omega) \tag{6}$$

with Fourier coefficients

$$\begin{aligned} a_1(\omega) &= \frac{2\omega}{\pi}\int_0^{\pi/\omega} u(t)\sin(\omega t)dt \\ b_1(\omega) &= \frac{2\omega}{\pi}\int_0^{\pi/\omega} u(t)\cos(\omega t)dt, \end{aligned} \tag{7}$$

where $u(t)$ denotes the output of $\mathcal{H}$ for $e := \sin(\omega t)$, *i.e.*, $\epsilon = 0$; for explicit expressions of the Fourier coefficients $a_1(\omega)$ and $b_1(\omega)$ in the case of HIGS from (1), see [5] and the references therein. Considering the configuration in Fig. 1, the describing function $\mathcal{N}^{\mathcal{C}_{\mathcal{H}}}$ for $\mathcal{C}^{\mathcal{H}}$ becomes

$$\mathcal{N}^{\mathcal{C}_{\mathcal{H}}}(j\omega) = \mathcal{N}^{\mathcal{H}}(j\omega)\left(\frac{\omega_i}{\omega_h}\cdot\frac{1}{|1+4j/\pi|} - \frac{j\omega_i}{\omega}\right). \tag{8}$$

In the Bode diagram of Fig. 2, for $\omega_i = \omega_h = 2\pi$ rad$\cdot$s^{-1}, $\mathcal{N}^{\mathcal{C}_{\mathcal{H}}}(j\omega)$ in (8) is shown (in red) together with the frequency response function of a simple (linear) integrator $\mathcal{C}(j\omega) = \omega_i/j\omega$ (in black). The figure shows that $\mathcal{N}^{\mathcal{C}_{\mathcal{H}}}(j\omega)$ has ampli-

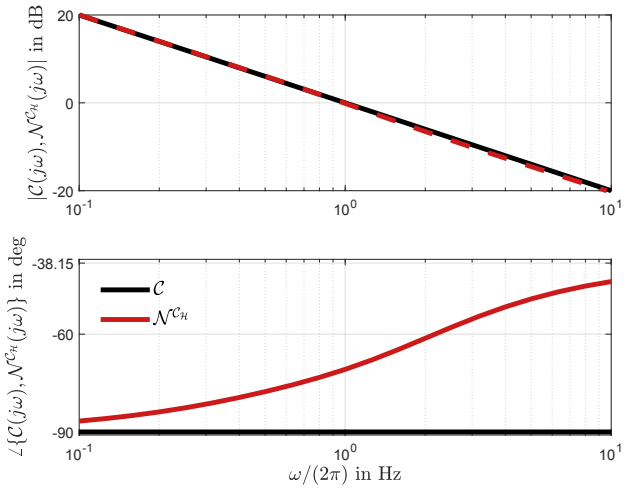

Fig. 2: Bode diagram of the describing functions $\mathcal{C}(j\omega)$, $\mathcal{N}^{\mathcal{C}_{\mathcal{H}}}(j\omega)$.

tude characteristics that approximately match the amplitude characteristics of the simple integrator $\mathcal{C}(j\omega)$, *i.e.*, having a slope of minus 20 dB per decade. However, the phase characteristics of $\mathcal{N}^{\mathcal{C}_{\mathcal{H}}}(j\omega)$ show a clear advantage in the sense of less phase lag than the minus 90 degrees associated with the linear integrator. In fact, the phase lag of $\mathcal{N}^{\mathcal{C}_{\mathcal{H}}}(j\omega)$ approaches -38.15 degrees for $\omega \to \infty$, which corresponds to the phase lag associated with a Clegg integrator [11]. The crossover frequency from -90 degrees of the linear integrator toward -38.15 degrees of a Clegg integrator is determined by ω_h and can be tuned almost independently from the amplitude characteristics, which is considered a useful feature of the HIGS design in Fig. 1.

IV. Problem description

For HIGS, the validity of the describing function $\mathcal{N}^{\mathcal{C}_{\mathcal{H}}}(j\omega)$ in (8), and its associated phase advantages, hinges crucially on the input signal e being harmonic. $\mathcal{H}$ is a nonlinear element that (in principle) does not support superposition. Its output satisfies $u(t, e_1 + e_2) \neq u(t, e_1) + u(t, e_2)$, where $u(t, e)$ denotes the response of $\mathcal{H}$ to input e with $e(0) = 0$. Therefore, one should be careful in using describing function analysis for non-harmonic input signals.

To illustrate this, consider the input e in (5) to the hybrid integrator $\mathcal{C}^{\mathcal{H}}$ from Fig. 1 with $\epsilon \in \{0, 1\}$. The resulting outputs u are shown in Fig. 3 at $f = 1$ Hz. The figure shows time-series simulations with the hybrid integrator $\mathcal{C}^{\mathcal{H}}$ (in red, 'HIGS') and with the simple integrator $\mathcal{C}(s) = \omega_i/s$ (in black, 'linear'). Both integrators are subject either to a

Authorized licensed use limited to: Eindhoven University of Technology. Downloaded on April 03,2023 at 18:16:04 UTC from IEEE Xplore. Restrictions apply.

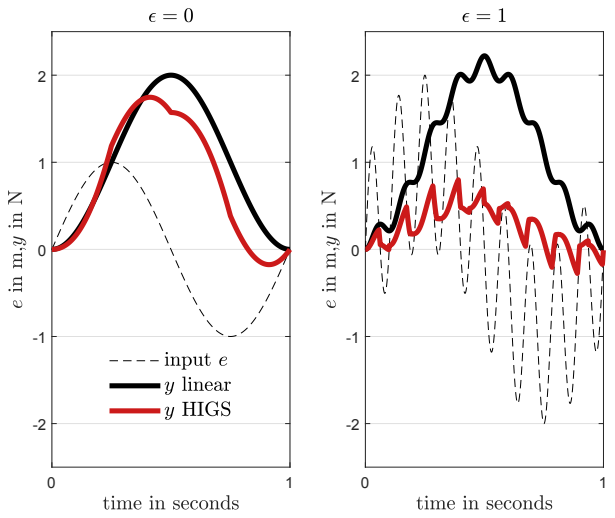

Fig. 3: Time series simulations of output y from $\mathcal{C}$ (black) or $\mathcal{C}^{\mathcal{H}}$ (red) to input e (dashed black); harmonic input (left, $\epsilon = 0$) versus multi-sine input (right, $\epsilon = 1$).

single harmonic input $e := e_1(t) = \sin(\omega t)$, *i.e.*, (5) with $\epsilon = 0$ (left figure), or a multi-sine input $e := e_1(t) + e_2(t)$, *i.e.*, (5) with $\epsilon = 1$ (right figure). For $\epsilon = 0$, it is clear that the hybrid integrator is able to generate an output $y(t, e_1)$ that contains mainly the frequency contents of the input e_1 at $f = 1$ Hz but with a phase advantage compared to the linear integrator. For $\epsilon = 1$, and due to superposition, the simple integrator captures the contribution at $f = 1$ Hz in its output irrespective of the presence of the additional contribution of the parasitic frequency component at $f = 9$ Hz. As such, $y(t, e_1+e_2) = y(t, e_1)+y(t, e_2)$. For the hybrid integrator $\mathcal{C}^{\mathcal{H}}$, however, the contribution at $f = 1$ Hz is not well captured. In fact, $\mathcal{H}$ in (1) is switching more frequently to gain mode due to the parasitic frequency component at $f = 9$ Hz, which limits integration of the 1 Hz component. The result is a gain loss by a factor 4 in the output y, clearly indicating that $y(t, e_1 + e_2) \neq y(t, e_1) + y(t, e_2)$.

As shown in the previous example, early switching to gain mode in the presence of high-frequency components will render the hybrid integrator less effective for the also present low-frequency components as a result of gain loss. As a consequence, low-frequency components, for which the integrator is designed to provide disturbance rejection, are less suppressed. This is shown in more detail in Fig. 4 by

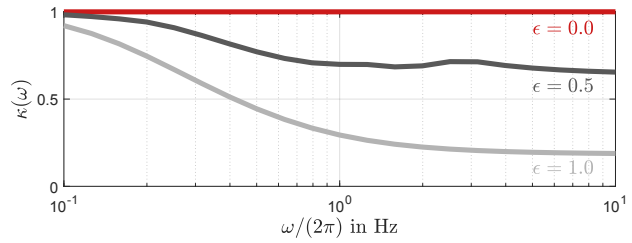

Fig. 4: Gain factor $\kappa(\omega)$ for $\mathcal{C}^{\mathcal{H}}$ with $\epsilon \in \{0, 0.5, 1\}$.

depicting the gain factor $\kappa(\omega)$, which is defined as

$$\kappa(\omega) = \left| \frac{\bar{a}_1(\omega) + j\bar{b}_1(\omega)}{a_1(\omega) + jb_1(\omega)} \right|, \tag{9}$$

with $\bar{a}_1(\omega), \bar{b}_1(\omega)$ the first Fourier coefficients obtained from taking the Fourier transform of output y, and $a_1(\omega)+jb_1(\omega)$ the describing function $\mathcal{N}^{\mathcal{C}_{\mathcal{H}}}(j\omega)$ in (8). For input e in (5), κ represents the magnitude of the frequency-dependent ratio between the actual first harmonic components in y to $e := e_1 + e_2$ with $\epsilon \in \mathbb{R}_{>0}$ and the ones predicted based on the describing function, for which it holds that $e := e_1$ with $\epsilon = 0$. In Fig. 4, it can be seen that $\epsilon > 0$ corresponds to smaller $\kappa(\omega)$ values at high frequencies. This associates with gain loss of $\mathcal{C}^{\mathcal{H}}$. The figure also shows that smaller values for ϵ, in this case $\epsilon = 0.5$, lead to more accurate approximation of the gain when using $\mathcal{N}^{\mathcal{C}_{\mathcal{H}}}(j\omega)$, because $\kappa \to 1$ for $\epsilon \to 0$. This is in line with the filter hypothesis [6] that admits small distortions of the harmonic input while still guaranteeing the validity of the describing function $\mathcal{N}^{\mathcal{C}_{\mathcal{H}}}(j\omega)$ in (8). Remark that in open loop and for some specific input signals, the solution $\kappa(\omega)$ can be found analytically. For general input signals, however, one needs to reside to numerical solutions.

V. Pre- and post-filtering

As a solution to the problem of gain loss in hybrid integrators under multi-sine input, we introduce pre- and post-filtering. Consider the filter configuration as depicted in Fig. 5, where the hybrid integrator $\mathcal{C}^{\mathcal{H}}$ from Fig. 1 is pre-

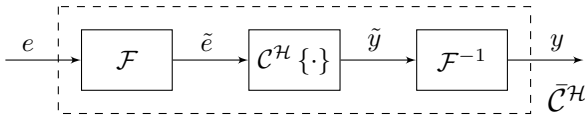

Fig. 5: Block diagram of $\bar{\mathcal{C}}^{\mathcal{H}}$ with pre- and post-filtering.

multiplied with transfer function $\mathcal{F}(s)$ and post-multiplied with the inverse $\mathcal{F}^{-1}(s)$ to obtain the modified HIGS configuration $\bar{\mathcal{C}}^{\mathcal{H}}$. Pre- and post-filtering assures that the loop transfer connecting the output y to the input e, which is generally determined by the plant and the additional linear controller part, remains unchanged. Stability properties of the closed-loop system thus remain unchanged. Note that we either assume that the inverse filter $\mathcal{F}^{-1}(s)$ is bi-proper, *i.e.*, $|\mathcal{F}^{-1}(s)| \to c_0$ for $\omega \to \infty$ and $c_0 \in \mathbb{R}_{\geq 0}$, or that we can approximate it by a (bi-)proper function $\tilde{\mathcal{F}}(s)$ such that $\|\mathcal{F}(s) \cdot \tilde{\mathcal{F}}(s) - 1\|_\infty \leq c_1$ with $0 < c_1 < 1$ sufficiently small. As a result of filtering the input e, the nonlinear operation $\mathcal{H}$ in (1) will use the filtered input $\tilde{e}$ instead and thus will induce a different nonlinear output $\tilde{y}$. The nonlinear distortion of the input signal by HIGS can be seen as the generation of (undesired) higher harmonics. The key point being that pre-filtering can avoid the nonlinear distortion to take place in HIGS, while pre- and post-filtering together preserve the properties of the loop transfer connected to HIGS. The post filter, subsequently, cannot amplify contributions that are no longer being generated. For $\mathcal{F}(s) \neq 1$, the post-filtering operation based on $\mathcal{F}^{-1}(s)$ will render the output y slightly different from $\tilde{y}$. Note that in the case of the simple integrator $\mathcal{C}(s) = \omega_i/s$ pre- and post-filtering is generally not useful,

Authorized licensed use limited to: Eindhoven University of Technology. Downloaded on April 03,2023 at 18:16:04 UTC from IEEE Xplore. Restrictions apply.

and that for the nonlinear integrator $\bar{\mathcal{C}}^{\mathcal{H}}$, pre- and post-filtering has no effect on the describing function $\mathcal{N}^{\mathcal{C}_{\mathcal{H}}}(j\omega)$ in (8).

To study the effect of the filtering approach in Fig. 5, consider the transfer function of a notch filter given by

$$\mathcal{F}(s) = \frac{s^2 + 2\beta_z \omega_{pp} s + \omega_{pp}^2}{s^2 + 2\beta_p \omega_{pp} s + \omega_{pp}^2} \tag{10}$$

with $\omega_{pp} = 9 \cdot 2\pi$ rad, $\beta_z = 0.01$, $\beta_p = 0.1$, and proper inverse $\mathcal{F}^{-1}(s)$. For $\epsilon \in \{0, 1\}$, the outputs y of $\bar{\mathcal{C}}^{\mathcal{H}}$ are shown in Fig. 6 at $f = 1$ Hz. Different from Fig. 3, Fig. 6

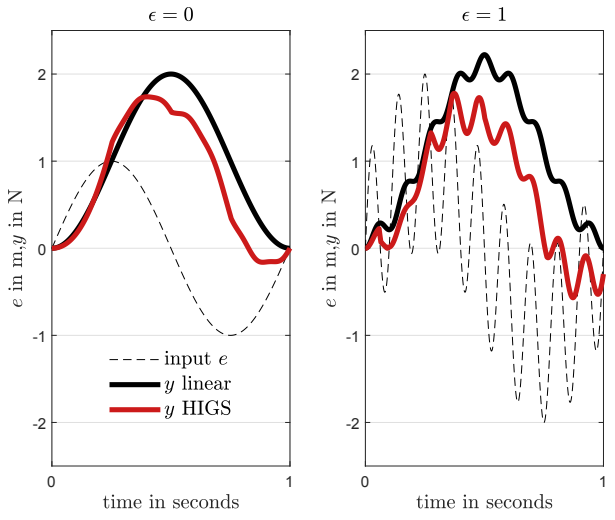

Fig. 6: Time series simulation of output y from $\mathcal{C}$ (black) or $\bar{\mathcal{C}}^{\mathcal{H}}$ (red) to input e (dashed black); harmonic input (left, $\epsilon = 0$) versus multi-sine input (right, $\epsilon = 1$).

does show for $\epsilon = 1$ the characteristic contribution at $f = 1$ Hz in the output y of the hybrid integrator.

The effect in terms of the gain factor $\kappa(\omega)$ for this new controller configuration is shown in Fig. 7. It can be seen that for $\epsilon \in \{0, 0.5, 1\}$ gain distortion remains within 5% of the gain expected from the describing function $\mathcal{N}^{\mathcal{C}_{\mathcal{H}}}$ in (8) and depicted in Fig. 2, thus effectively solving for the problem of gain loss. Namely, filtering the parasitic contribution at 9 Hz in e from (5) with the notch filter from (10) induces a filtered input $\tilde{e}$ to $\mathcal{H}(\cdot)$ that is highly harmonic and thus preserves the contribution at 1 Hz in its output $\tilde{y}$. The output y, however, does slightly differ from the hybrid integrator output $y := \tilde{y}$ with $\epsilon = 0$ and $\mathcal{F}(s) = 1$. This is mainly because $\mathcal{H}$ does generate contributions at 9 Hz, so-called nonlinear distortions, that are amplified by $\mathcal{F}^{-1}(s)$ when using (10). This also explains why the curve of $\kappa(\omega)$ at $\epsilon = 0$ no longer resembles a straight line with gain one as was the case with $\mathcal{C}^{\mathcal{H}}$ in Fig.4.

The choice for pre- and post-filters is not restricted to the example in (10). In practice, the input e is generally non-harmonic and may contain an arbitrary amount of frequency components. Other filters like skew notch, lowpass or the bandpass-type may then provide a more appropriate choice. Regardless the choice of filters, the design philosophy remains the same: $\mathcal{F}(s)$ is chosen such that the filtered input signal $\tilde{e}$ triggers the switching behavior of $\mathcal{C}^{\mathcal{H}}$ in a desired

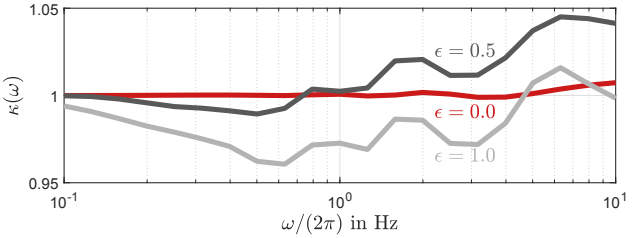

Fig. 7: Gain factor $\kappa(\omega)$ for $\bar{\mathcal{C}}^{\mathcal{H}}$ with $\epsilon \in \{0, 0.5, 1\}$.

manner. Also, the justification for applying the operation $\mathcal{F}^{-1}(s)$ on output $\tilde{y}$, which could lead to amplification of higher harmonics, should be in accordance with the filter hypothesis. This renders the choice for pre- and post-filters dependent on (i) the system, (ii) the controller configuration/arrangement, and (iii) the spectral properties of the exogenous inputs.

VI. Case Study on a Wafer Stage System

In order to demonstrate the effectiveness of pre- and post-filtering in a HIGS-PID control design, consider the example of a wafer scanner. Wafer scanners arguably perform one of the most challenging steps in the production of microchips, namely exposing a chip topology obtained from a reticle onto the photo-resistive layers of a silicon wafer. For a general description of the control of wafer scanners, see [1].

Here, we focus on the servo control of the short-stroke wafer stage in scanning y-direction. A simplified motion control scheme is depicted in Fig. 8, where the wafer stage

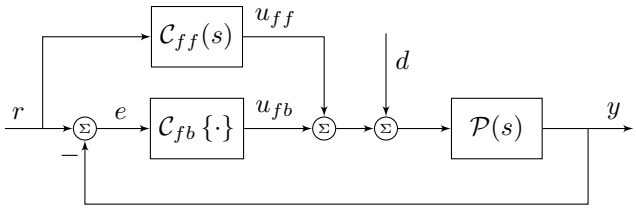

Fig. 8: Block scheme of a controlled wafer stage.

plant is represented by $\mathcal{P}(s)$, the input to the plant consists of a force disturbance d, and two control signals u_{ff} and u_{fb}, while the measured output y is subtracted from the reference r to form the feedback error signal e; the reference r is input to the feedforward controller $\mathcal{C}_{ff}(s)$, which is designed to approximate the inverse of $\mathcal{P}(s)$, and which is needed to achieve nano-scale tracking performance under acceleration levels up to 45 m/s^2; the servo error signal e is input to the feedback controller $\mathcal{C}_{fb}\{\cdot\}$ and is designed to achieve disturbance rejection under robust stability constraints.

For wafer stage feedback control, it is common practice to use a linear controller of the form

$$\mathcal{C}_{fb}(s) = \mathcal{C}_{pid}(s)\mathcal{C}_{lp}(s)\prod_{i=1}^{4}\mathcal{C}_{n,i}(s), \tag{11}$$

i.e., the series interconnection of a PID filter

$$\mathcal{C}_{pid}(s) = k_p\left(1 + \frac{\omega_i}{s} + \frac{s}{\omega_d}\right) \tag{12}$$

Authorized licensed use limited to: Eindhoven University of Technology. Downloaded on April 03,2023 at 18:16:04 UTC from IEEE Xplore. Restrictions apply.

with gain k_p and corner frequencies ω_i and ω_d for its integrator and differentiator, respectively, a second-order lowpass filter of the form

$$\mathcal{C}_{lp}(s) = \frac{\omega_{lp}^2}{s^2 + 2\beta\omega_{lp}s + \omega_{lp}^2} \tag{13}$$

with cut-off frequency ω_{lp} and dimensionless damping coefficient β, and multiple notch filters of the form

$$\mathcal{C}_{n,i}(s) = \left(\frac{\omega_p^2}{\omega_z^2}\right)\left(\frac{s^2 + 2\beta_z\omega_z s + \omega_z^2}{s^2 + 2\beta_p\omega_p s + \omega_p^2}\right),\ i \in \{1,2,3,4\} \tag{14}$$

with ω_z, ω_p the frequencies associated with the zeros and poles, respectively, and β_z, β_p the corresponding (dimensionless) damping coefficients. With the purpose of providing an intuitive feeling for the performance level that is common for an industrial wafer stage feedback control system, the (measured) input sensitivity function $\mathcal{S}(j\omega) = (1 + \mathcal{C}_{fb}(j\omega)\mathcal{P}(j\omega))^{-1}$ of a representative robust linear control design is shown in Fig. 9 (black curve) by means of its magnitude characteristics. The frequency response functions

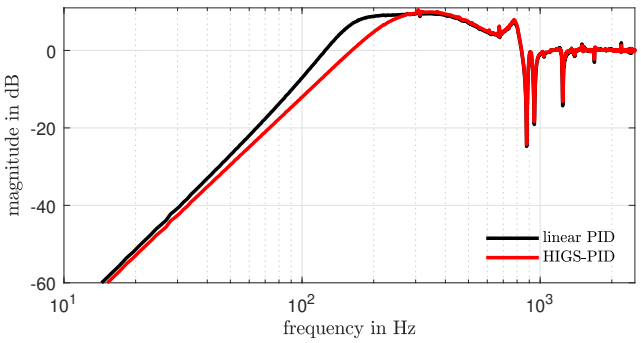

Fig. 9: Bode magnitude plots of the sensitivity functions with linear PID control (black) and HIGS-PID control (red).

are obtained (partly) from closed-loop identification of the sampled data system with a sampling frequency of 5 kHz and associate with a bandwidth (magnitude of the open-loop frequency response at 0 dB) of 236 Hz.

Let us also adopt a hybrid PID controller $\mathcal{C}_{fb}^{\mathcal{H}}$ in a similar manner as (11) but with the difference that the integrator in $\mathcal{C}_{pid}(s)$ in (12) is replaced by the respective HIGS counterpart such as discussed in Section III. A frequency-domain representation of $\mathcal{C}_{fb}^{\mathcal{H}}$ is given (in an approximative sense) by the describing function

$$\mathcal{N}_{fb}^{\mathcal{H}}(\bar{s}) = \mathcal{C}_n(\bar{s})\mathcal{N}_{pid}^{\mathcal{H}}(\bar{s})\mathcal{C}_{lp}(\bar{s}) \text{ with } \bar{s} = j\omega, \tag{15}$$

with

$$\mathcal{N}_{pid}^{\mathcal{H}}(\bar{s}) = k_p\left(1 + \mathcal{N}^{\mathcal{C}_{\mathcal{H}}}(\bar{s}) + \frac{\bar{s}}{\omega_d}\right) \tag{16}$$

the describing function of the HIGS-PID filter. Note that $\mathcal{N}^{\mathcal{C}_{\mathcal{H}}}(\bar{s})$ refers to (8) with $\omega_h = \omega_i = 100 \cdot 2\pi$ rad/s. Similar to the linear controller, the hybrid PID controller is tuned for maximum bandwidth, in this case 280 Hz, while satisfying robust stability constraints. Differently, however, these constraints are embedded in a quasi-linear loop-shaping procedure that exploits the describing function from (15); see for example [5]. The resulting quasi-linear input sensitivity function $\mathcal{S}^{\mathcal{H}}(j\omega) = (1 + \mathcal{N}_{fb}^{\mathcal{H}}(j\omega)\mathcal{P}(j\omega))^{-1}$ is also depicted in Fig. 9 and indicated by the red curve. It is important to realize that the pre- and post-filters as discussed in Section V cancel out in (15), and, therefore, do not affect the characteristics of $\mathcal{S}^{\mathcal{H}}(j\omega)$ such as shown in Fig. 9. Note also that although the bandwidth with hybrid PID control is increased from 236 Hz to 280 Hz, the phase advantages of the HIGS integrator are mainly exploited for $\omega \leq \omega_i < \omega_{bw}$. In fact, around the bandwidth $\omega \approx \omega_{bw}$ the controlled wafer stage represents a double-integrator system that still needs D-action to obtain proper encirclement of the point $(-1, 0)$. Though, with hybrid PID control such a D-action can typically be shifted toward higher frequencies, *i.e.*, inducing less amplification of high-frequency noise.

A. Measurement results: without pre- and post-filtering

To study the results of pre- and post-filtering through time-domain measurement results, we first focus on the case without pre- and post-filtering, *i.e.*, Fig. 5 with $\mathcal{F}(s) = 1$. By evaluating the cumulative power spectral densities of the measured closed-loop signals e with either the linear PID control design (in black) or the HIGS-PID control design (in dashed red), Fig. 10 shows inferior low-frequency

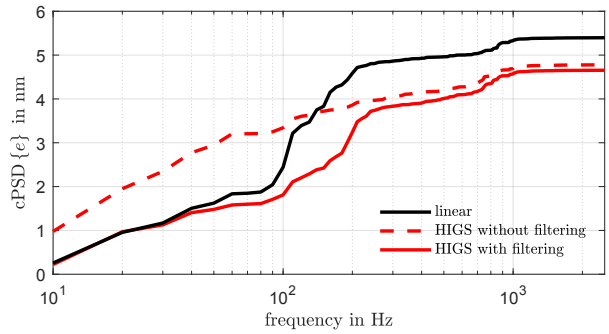

Fig. 10: Measured cumulative power spectral densities (cPSD) of the servo error $e(t)$ with or without pre- and post-filtering.

disturbance rejection properties for the hybrid PID control design. In the comparison the exogenous input r, *i.e.*, the setpoint, is highly reproducible and constitutes for the main part of the frequency contents in e despite the presence of an appropriate feedforward control design. This is different for the exogenous input d that stems from multiple noise sources and that is generally non-reproducible. Its contribution however constitutes a minor part of the frequency contents in e. The result shown in Fig. 10 is not in accordance with the sensitivity analysis from Fig. 9. The discrepancy between linear PID and HIGS-PID performance without filtering is particularly visible at low frequencies. In fact, a significant gain loss is found in the frequency range below 200 Hz. Observe that gain loss is not evaluated as done previously through κ in (9), because the measurement results refer to data resulting from tracking a wafer scanning profile, which is done using a non-periodic input. In accordance with the discussion from Section IV, it is hypothesized that frequency

Authorized licensed use limited to: Eindhoven University of Technology. Downloaded on April 03,2023 at 18:16:04 UTC from IEEE Xplore. Restrictions apply.

contributions in e above 200 Hz induce too-frequent switching (or chattering) of the hybrid PID controller to gain mode. This is supported by Fig. 11, which depicts time-domain

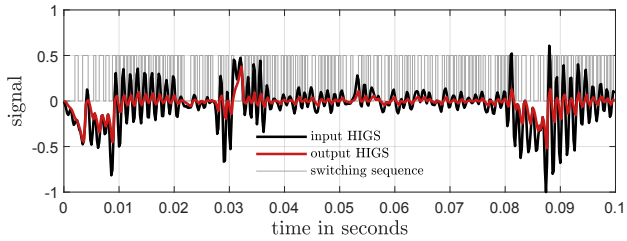

Fig. 11: Time-domain measurements of HIGS' input (black) and output (red) for the HIGS-PID controller without pre- and post filtering.

measurements of the input and output signals of $\mathcal{H}$ in (1) and associated with the HIGS in the PID controller. It can be seen that switching between integrator mode and gain mode occurs for the HIGS-PID controller at a frequency of about 750 Hz, which is too high for the integrator to be effective for disturbances below 200 Hz.

B. Measurement results: with pre- and post-filtering

As a solution to gain loss consider the hybrid PID control design with pre- and post-filtering in which $\mathcal{F}(s)$ from Fig. 5 is chosen as a second-order lowpass filter of the form

$$\mathcal{F}(s) = \frac{\omega_{pp}^2}{s^2 + 2\beta_p\omega_{pp}s + \omega_{pp}^2} \tag{17}$$

with $\omega_{pp} = \omega_h^i$, $\beta_p = 1$. The inverse of (17) is non-proper, but can be approximated by a (bi-proper) skew notch filter with its poles placed at a higher frequency than its zeros. The choice for (17) is motivated by the design argument to let the HIGS-PID controller operate (and thus switch) on frequency content below 200 Hz. Of course, the mitigation of the problem with $F(s)$ is less effective should either the exogenous inputs r, d have more high-frequency components or the existing high-frequency components become more dominant. In this sense the choice for $F(s)$ depends on the considered application.

In Fig. 10, also the result of hybrid PID control with pre- and post-filtering is shown through the solid red curve. It can be seen that the result is well in line with the expectations raised from the sensitivity plots from Fig. 9. This demonstrates that the describing function-based sensitivity function for the considered wafer stage example only provides an accurate frequency-domain reflection of the nonlinear closed-loop system behavior for the case of pre- and post-filtering. It should be remarked that tuning of the parameters ω_{pp}, β_p toward robust performance is done in the time domain, based on the spectral content of e.

For the given pre- and post-filters, Fig. 12 shows the measured time-series of the input and output signals of $\mathcal{H}$ in (1) and associated with the HIGS-PID controller. It can be seen that switching between integrator mode and gain mode for the HIGS-PID controller is (i) well-balanced between both modes, (ii) at a sufficiently low rate, and (iii) with the appropriate spectral content, when compared to Fig. 11.

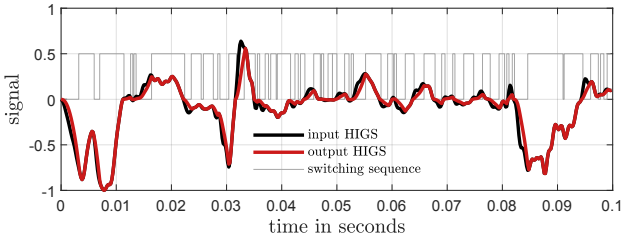

Fig. 12: Time-domain measurements of HIGS' input (black) and output (red) for the HIGS-PID controller with pre- and post filtering.

VII. Conclusions

Improved low-frequency disturbance rejection with hybrid integrators hinges on the distribution of the spectral content in the input signal to the HIGS elements. The presence of dominating high-frequency components may induce too-frequent switching to gain mode, which results in gain loss of its simple integrator. A solution to overcome gain loss in hybrid control designs is proposed in the form of pre- and post-filtering. Appropriate selection and tuning of the pre- and post-filters allows for a well-balanced switching behaviour of HIGS, restoring its gain to the level obtained from first-order describing function analysis. Wafer stage measurement results demonstrate the need for pre- and post-filtering in practice for increased effectiveness of the HIGS-PID design on low-frequency disturbance rejection.

References

[1] H. Butler. (2011) Position control in lithographic equipment. IEEE Control Systems Magazine, 31(5) pp. 28-47.

[2] L. Chen, N. Saikumar, H. Hossein Nia Kani. (2019) Development of robust fractional-order reset control. IEEE Transactions on Control Systems Technology, 28(4), pp. 1404-1417.

[3] D.A. Deenen, M.F. Heertjes, W.P.M.H. Heemels, and H. Nijmeijer. (2017) Hybrid integrator design for enhanced tracking in motion control. In Proc. American Control Conference, Seattle, pp. 2863-2868.

[4] S.J.A.M. van den Eijnden, Y. Knops, M.F. Heertjes. (2018) A hybrid integrator-gain based low-pass filter for nonlinear motion control, In Proc. Conference of Control Technology and Applications, Copenhagen, Denmark, pp. 1108-1113.

[5] S.J.A.M. van den Eijnden, M.F. Heertjes, H. Nijmeijer. (2020) Experimental Demonstration of a Nonlinear PID-Based Control Design Using Multiple Hybrid Integrator-Gain Elements. Proc. American Control Conference, Denver, pp. 4307-4312.

[6] A. Gelb, W.E. Vander Velde. (1968) Multiple-Input Describing Functions and Nonlinear System Design. McGraw-Hill, New York.

[7] M.F. Heertjes, X.G.P. Schuurbiers, H. Nijmeijer. (2009) Performance-improved design of N-PID controller motion systems with applications to wafer stages. IEEE Transactions on Industrial Electronics, 56(5), pp. 1347-1355.

[8] B.G.B. Hunnekens, N. van de Wouw, H. Nijmeijer. (2012) Variable gain motion control for transient performance improvement. Proc. American Control Conference (ACC), Montréal, pp. 2467-2472.

[9] R.W. Schafer, A.V. Oppenheim, T.G. Stockham. (1968) Nonlinear filtering of multiplied and convolved signals, Proc. IEEE, vol. 56, no. 8, pp. 1264–1291.

[10] B. Sharif, A. van der Maas, N. van de Wouw, and W.P.M.H. Heemels. (2021) Filtered Split-Path Nonlinear Integrator: A Hybrid Controller for Transient Performance Improvement, IEEE Transactions on Control Systems Technology, accepted for publication.

[11] L. Zaccarian, D. Nešić, and A.R. Teel. (2005) First order reset elements and the Clegg integrator revisited. Proc. American Control Conference (ACC), Portland, pp. 563–568.

[12] J. Zhang, K.H. Johansson, J. Lygeros, S. Sastry. (2001) Zeno hybrid systems. J. of Robust and Nonlinear Control, 11, pp. 435-451.

Authorized licensed use limited to: Eindhoven University of Technology. Downloaded on April 03,2023 at 18:16:04 UTC from IEEE Xplore. Restrictions apply.